Sensors & Actuators: B. Chemical 320 (2020) 128324

Contents lists available at ScienceDirect

Sensors and Actuators B: Chemical

journal homepage: www.elsevier.com/locate/snb

# A signal-off electrochemical sensing platform based on $Fe_3S_4$-Pd and pineal mesoporous bioactive glass for procalcitonin detection

Liu Qu[a], Lei Yang[a], Yong Ren[b], Xiang Ren[a], Dawei Fan[a], Kun Xu[a,c], Huan Wang[a,*], Yueyuan Li[a,*], Huangxian Ju[a], Qin Wei[a]

[a] Collaborative Innovation Center for Green Chemical Manufacturing and Accurate Detection, Key Laboratory of Interfacial Reaction & Sensing Analysis in Universities of Shandong, School of Chemistry and Chemical Engineering, University of Jinan, Jinan 250022, PR China
[b] Department of Mathematical Sciences, Zibo Normal College, Zibo, Shandong 255130, PR China
[c] Anhui Dexinjia Biopharm Co., Ltd., Fuyang, 236600, PR China

ARTICLE INFO

*Keywords:*
Sandwich-type immunosensor
Signal-off mode
Magnetic $Fe_3S_4$-Pd
Pineal mesoporous bioactive glass
Procalcitonin

ABSTRACT

Herein, a sandwich-type electrochemical (EC) immunosensor is proposed based on a special signal-off mode for the sensitive detection of procalcitonin (PCT) by utilizing $Fe_3S_4$ loaded with Pd nanoparticles ($Fe_3S_4$-Pd) as a signal indicator and matrix and functionalized pineal mesoporous bioactive glass (PBG) as the label for signal amplification. $Fe_3S_4$-Pd not only shows excellent electrocatalytic activity for the $H_2O_2$ redox reaction but is also firmly immobilized on a magnetic glassy carbon electrode due to its excellent magnetic properties; because of the above features, this immunosensor exhibits excellent sensitivity and stability, respectively. Glutaraldehyde is used as a cross-linking agent to bond the secondary antibodies ($Ab_2$) with PBG. It is worth mentioning that the electron transfer rate between the electrolyte and electrode is decreased significantly by PBG-$Ab_2$; thus, a sensitive variation in the current signal is observed, and a further improvement in the sensitivity of the immunosensor is realized. More importantly, the proposed signal-off sensing system has a wide linear detection range of 500 fg/mL to 50 ng/mL for PCT and a low detection limit of 130 fg/mL, which promotes it as a promising detection method for the sensitive detection of other biomarkers.

## 1. Introduction

Sepsis is a syndrome of organ dysfunction that can be life-threatening in severe cases [1], and recently, it has become a frequent cause of severe disease and death around the world [2]. The detection of procalcitonin (PCT), which is a biomarker of sepsis, has been widely considered due to its benefit for early diagnosis in critically ill patients [3]. Thus, a sensitive recognition and accurate quantification of PCT in serum is crucial for an effective early diagnosis and to further guide sepsis treatment. To date, many detection strategies have been adopted for PCT determination, such as enzyme-linked immunosorbent assays [4], chemiluminescence immunoassays [5] and lateral flow immunoassays [6]. However, their low sensitivity and narrow linear range make the detection of trace PCT in human serum very difficult. Compared with the above methods, an electrochemical (EC) immunosensor is a promising instrument with the advantages of high sensitivity, fast response time, miniaturization, and low cost, along with point-of-care applications that can promote a new dawn for the sensitive detection of PCT [7–9]. Meanwhile, in recent years, representative achievements have been made in the research of EC sensing based on different amplification strategies, such as competitive type, label-free type and sandwich-type EC immunosensors, including signal-on and signal-off strategies, which has further greatly improved the sensitivity and promoted the development of EC immunosensor [10–12].

Due to their high catalytic activity, in recent years, various types of nanozymes, such as metal oxides, metal sulfides, and noble metal nanoparticles, have generally been used in the field of EC immunosensors [13–15]. It is known that iron-based sulfide has many characteristics, for example, FeS and $FeS_2$ exhibit superior removal capacity for divalent heavy metal ions and $Fe_3S_4$ acts as a potential anode material in lithium-ion batteries [16,17]. Furthermore, $Fe_3S_4$ has an equally good magnetic performance as its precursor, $Fe_3O_4$ [18,19]. Therefore, the above advantages have opened up broad application prospects for $Fe_3S_4$ in biomedicine, electrochemistry and other fields [20]. Moreover, the significant half-metallic magnetic material $Fe_3S_4$ contains $Fe^{2+}$ and $Fe^{3+}$ oxidation states on the lattice surface, which endow it with unique catalytic properties [21]. Thus, $Fe_3S_4$ as a kind of nanozyme has been taken into consideration. While, the surface modification of nanozymes

* Corresponding authors.
*E-mail addresses:* wanghuan8711@163.com (H. Wang), yueyuanli86@163.com (Y. Li).

https://doi.org/10.1016/j.snb.2020.128324
Received 9 March 2020; Received in revised form 14 May 2020; Accepted 17 May 2020

with established nanotechnology can significantly improve their catalytic performance and enhance the sensitivity of the immunosensor [22,23]. It has been reported that Pd NPs have unique catalytic activity, for example, Pd NP-loaded homochiral covalent organic frameworks can be used for heterogeneous asymmetric catalysis; additionally, an oleylamine-mediated synthesis of Pd NPs can be used for the catalysis of formic acid oxidation [24,25]. Therefore, compared with some other non-precious catalysts, heterogeneous enzyme-like biomimetic catalysts, synthase and artificial enzyme, the nanocomposite enzyme $Fe_3S_4$-Pd formed by loading Pd NPs on the surface of $Fe_3S_4$ has a broader application prospect in improving the catalytic activity of $H_2O_2$ [26,27].

To achieve a more sensitive detection of PCT, a type of mesoporous bioactive glass (MBG), pineal MBG (PBG) can be applied as an electron blocking label in the construction of the immunosensor. PBG possesses a high impedance. Additionally, PBG possesses high biocompatibility and a large specific surface area that promotes its extensive application in the clinical medicine and biosensor fields [28,29].

In our present work, after a large amount of Pd NPs were uniformly connected to the uneven surface of $Fe_3S_4$ by an in situ reduction, $Fe_3S_4$-Pd, which demonstrated a high catalytic performance, was formed as the signal indicator; thus, the sensitivity was enhanced by improving the current signal toward the catalytic reduction of $H_2O_2$. Moreover, the strong magnetic interaction between $Fe_3S_4$-Pd and a magnetic glass carbon electrode (MGCE) enabled it to be firmly fixed, which greatly improved the stability of the immunosensor. For improving the sensitivity further, a high-resistance coupling agent glutaraldehyde (GA) was utilized to connect PBG-$NH_2$ with $Ab_2$. In addition, its large specific surface could increase the loading amount of dielectric $Ab_2$ [30]. The resistance of the PBG-GA-$Ab_2$ (PBG-$Ab_2$) label was greatly enhanced due to the hindrance to the electron transfer from high-resistance GA and non-conductive $Ab_2$. Hence, based on the above observations, a signal-off EC sensing platform was proposed based off measuring the sensitive variation of the current signal. In this way, an obvious signal amplification was realized, which more effectively improved the sensitivity and provided a feasible method for clinical testing.

## 2. Experimental section

### 2.1. Apparatus and reagents

The apparatus and reagents in this work are described in the *Supporting Information*. All the water used in the experiment was ultrapure water.

### 2.2. Synthesis of $Fe_3S_4$

$Fe_3S_4$ was synthesized by following the procedure in reports [31]. $Fe_3O_4$ as a precursor of $Fe_3S_4$ was first synthesized, which is described in the *Supporting Information*. Then, the prepared $Fe_3O_4$ (0.025 g) was mixed with thioacetamide (0.23 g) and dispersed in 30 mL of ethanol. After stirring for 30 min, the solution was heated to 120 °C for 10 h. Finally, the mixture was treated with a magnetic separation washing method and dried in vacuum at 35 °C to obtain a black powder.

### 2.3. Synthesis of $Fe_3S_4$-Pd

The preparation of $Fe_3S_4$-Pd was conducted with the following steps: $Na_2PdCl_4$ solution (0.01 mmol/L, 60 mL) was mixed with a solution of $Fe_3S_4$ (2 mg/mL, 15 mL), and the mixture was subjected to ultrasonication to ensure that the sample was fully mixed. Then, a $NaBH_4$ (0.1 mol/L, 60 mL) solution was added dropwise into the mixture with mechanical stirring for 2 h. The final black precipitate of $Fe_3S_4$-Pd was separated and washed using water and absolute ethanol by a magnetic separation washing method.

### 2.4. Synthesis of PBG-$NH_2$

PBG was synthesized according to the previously reported literature of Liang [32]. Microemulsion droplets prepared from ethyl acetate (EA) and hexadecy ltrimethyl ammonium bromide (CTAB) were used as the soft template for synthesis of spherical MBG (SBG) precursors. First, 0.7 g CTAB was dissolved completely in 33 mL ultrapure water under stirring at 30 °C, and 10 mL of EA was added into the solution. After approximately 30 min, the successful formation of microemulsion droplets was observed, and 7 mL of aqueous ammonia (3 mol/L) was subsequently added. The mixture was stirred for another 15 min, and then 3.6 mL of tetraethyl orthosilicate, 0.36 mL of triethyl phosphate and 2.3 g of calcium nitrate tetrahydrate were sequentially added into the above mixture at 30 min intervals. Finally, the mixture was stirred well and transferred into a Teflon-lined autoclave, heated at 100 °C for 20 h under autogenous pressure. After the reaction, the white precipitate was washed three times with absolute ethanol and water, collected by centrifugation and dried at 60 °C for 24 h. Eventually, the final PBG samples were calcined at 650 °C in an air atmosphere to remove organics and nitrates.

PBG-$NH_2$ was synthesized as follows [28]. Briefly, the synthesized PBG (100 mg) was dispersed in anhydrous toluene (50 mL), thoroughly mixed, and preheated to 60 °C in an oil bath under stirring. After dropwise adding (3-aminopropyl) triethoxysilane (APTES, 1 mL), a reflux reaction was maintained for 6 h with magnetic stirring. Then, the unreacted APTES was removed by centrifugation (5000 rpm) for 5 min. After pouring off the supernatant, the precipitate was washed three times with anhydrous toluene. Finally, the washed precipitate was dried overnight.

### 2.5. Preparation of PBG-Au-$Ab_2$, PBG-EDC/NHs-$Ab_2$ and PBG-GA-$Ab_2$

In this work, Au NPs, EDC/NHs and GA were used as cross-linking agents to connect PBG-$NH_2$ and $Ab_2$, and PBG-Au-$Ab_2$, PBG-EDC/NHs-$Ab_2$ and PBG-GA-$Ab_2$ were prepared, respectively. The preparation process of Au NPs was listed in the *Supporting Information*. The $Ab_2$ solution (10 μg/mL, 500 μL) was added to the prepared PBG-$NH_2$ solution (4 mg/mL, 500 μL), followed by the addition of cross-linking agents Au NPs (10 mL), EDC (2 mmol/L, 500 μL) and NHs (10 mmol/L, 500 μL) and GA (2.5 wt%, 200 μL), respectively. Then the three mixtures were incubated at 4 °C overnight, and the resulting PBG-Au-$Ab_2$, PBG-EDC/NHs-$Ab_2$ and PBG-GA-$Ab_2$ were centrifuged, redispersed in PBS solution (pH = 7.4, 1 mL), and stored at 4 °C for further use.

### 2.6. Fabrication of the EC immunosensor

The proposed sandwich-type EC immunosensor was fabricated as illustrated in Fig. 1. MGCE with a 4 mm diameter was sequentially polished to a mirror-like finish using alumina slurries with different granularities (1.0, 0.3 and 0.05 μm). Next, the MGCE was washed thoroughly and dried with flowing nitrogen. First, a uniformly dispersed solution of $Fe_3S_4$-Pd (1.2 mg/mL, 6 μL) was dripped onto the MGCE, and due to the magnetic interaction between the MGCE and $Fe_3S_4$-Pd, a firm immobilization of the matrix was guaranteed. After drying at room temperature, the electrode was dipped with $Ab_1$ (10 μg/mL, 6 μL) and incubated at 4 °C for 1 h. After washing, bovine serum albumin (BSA, 0.1 wt%, 3 μL) was blocked on the surface of the electrode at room temperature for 1 h to block nonspecific binding sites. After being washed with PBS, the electrode could be incubated to recognize varying concentrations of PCT (500 fg/mL ~ 50 ng/mL) for 1 h at room temperature. Then, the electrode was washed thoroughly to remove unbound PCT molecules. Eventually, 6 μL of the prepared PBG-$Ab_2$ solution was immobilized onto the above electrode for 1 h at room temperature. Finally, after being washed with PBS to remove nonspecifically bound PBG-$Ab_2$, the proposed immunosensor was ready for measurement tests.

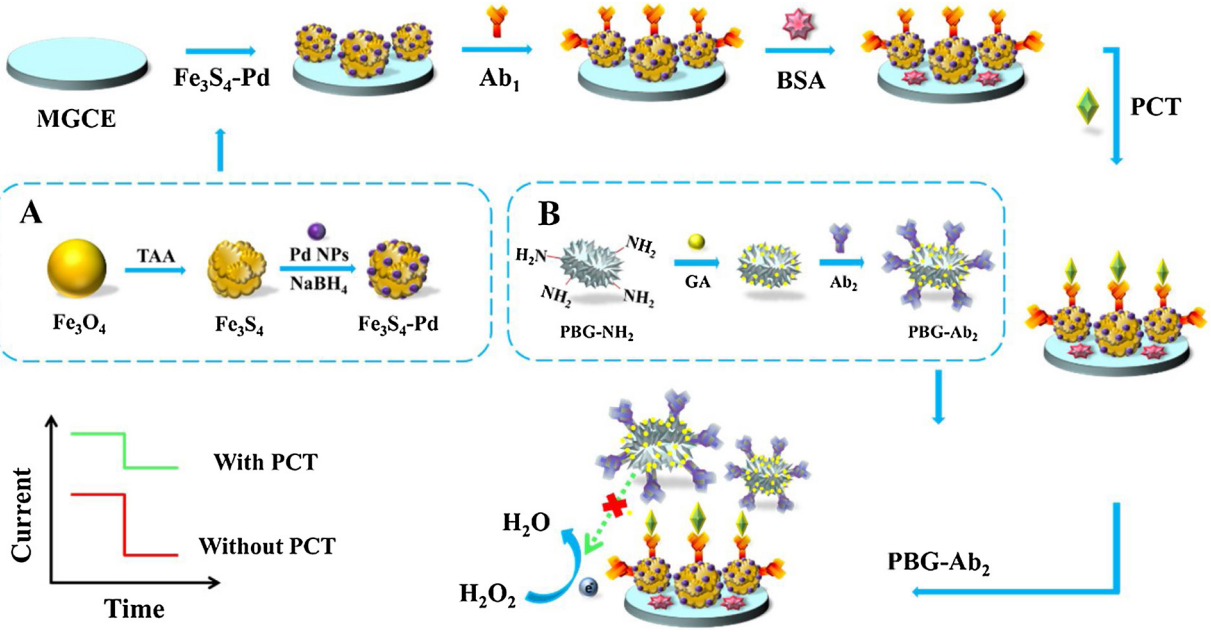


**Fig. 1.** Schematic presentation showing the fabrication process of the EC immunosensor: (A) preparation of $Fe_3S_4$-Pd and (B) preparation of PBG-$Ab_2$.

### *2.7. Experimental measurements*

An amperometric *i-t* curve method was employed in the process of testing the fabricated immunosensor. Under a scanning potential of -0.4 V, the background signal gradually stabilized, and then $H_2O_2$ (5 mol/L, 10 μL) was injected into the PBS solution under intense stirring.

## 3. Results and discussion

### *3.1. Characterization of the prepared materials: $Fe_3S_4$-Pd and PBG-$NH_2$*

The X-ray powder diffraction (XRD) patterns of $Fe_3O_4$, $Fe_3S_4$ and $Fe_3S_4$-Pd are shown in Fig. 2A. From the XRD pattern (curve a), all peaks could be fitted to crystalline $Fe_3O_4$ (JCPDS card No. 26-1136). Compared with the $Fe_3O_4$ precursor, the characteristic peak position of $Fe_3S_4$ changed after vulcanization. The diffraction peaks in the XRD pattern (curve b) were fully consistent with cubic greigite $Fe_3S_4$ (JCPDS card No. 89-1998). After the modification with Pd NPs, additional peaks could be observed in the XRD pattern (curve c) and were indexed to the Pd (111), (200) and (220) planes. The morphology of the materials was observed by scanning electron microscopy (SEM) and compared with the $Fe_3O_4$ precursor (Fig. 2B). $Fe_3S_4$ (Fig. 2C) is a spherical-like structure with a more rugged surface. As shown in Fig. 2D, Pd NPs had a good distribution on the surface of $Fe_3S_4$, and the energy dispersive spectrometer (EDS) images (Fig. S1) further indicated the successful attachment of Pd NPs. High-resolution X-ray photoelectron spectroscopy (XPS) was used to continuously ascertain the presence of Fe and S and their valence states in $Fe_3S_4$ (Fig. 2E–G). The narrow peaks at 713.2 and 726.5 eV matched the diagnostic peaks for $Fe^{3+}$ ions, and the other two peaks at 711 and 724.5 eV belonged to $Fe^{2+}$ species (Fig. 2F) [33,34]. The smooth peaks of the S 2p spectrum (Fig. 2G) at 163.5 and

165.1 eV were assigned to $S^{2-}$ ions [33,35]. Based on the above XRD, SEM and XPS results, the synthesis of $Fe_3O_4$, $Fe_3S_4$ and $Fe_3S_4$-Pd was successful.

As illustrated by SEM (Fig. 2H) and transmission electron microscopy (TEM) (Fig. 2I), the PBG nanoparticles showed a pinecone-like morphology. The pores, due to corrosive, could be clearly observed from the surface to the interior of the PBG. The average diameter of PBG was approximately 150 nm. According to the energy-dispersive X-ray (EDX) mapping of PBG, it was apparently composed of Ca, O, Si and P. The XRD patterns confirmed the amorphous phase of the PBG nanoparticles (Fig. S2). Through the Brunauer-Emmett-Teller (BET) technique (Fig. 2K), the specific surface area and the total pore volume were measured to be 367.40 $m^2/g$ and 1.08 $cm^3/g$, respectively. A large pore size distribution of approximately 38 nm could be observed, which resulted from the slit-shaped pores of the PBG materials as shown in the TEM images (Fig. 2I). FTIR spectra of the PBG-$NH_2$ nanoparticles revealed N-H vibration bands characteristic of $NH_2$ functional groups (Fig. 2L). Compared with pure PBG (curve a), PBG-$NH_2$ (curve b) exhibited two new peaks at 1580 $cm^{-1}$ and 680 $cm^{-1}$, which were attributed to the stretching vibrations of N—H in the amino groups from APTES [36]. The above data verified that the amine group was successfully grafted to PBG. All of the results indicated that the preparation of PBG and PBG-$NH_2$ in this work was successful.

### *3.2. EC characterization of the immunosensor*

Cyclic voltammetry (CV) was performed in a 5 mmol/L $K_3[Fe(CN)_6]$ solution to investigate the charge-transfer efficiency of $Fe_3S_4$-Pd and confirm the successful linkage of $Ab_1$. As illustrated in Fig. S3, when compared with $Fe_3S_4$ (curve b), $Fe_3S_4$-Pd (curve c) presented a higher EC response signal due to the large loading of Pd NPs, which obviously improved the conductivity of $Fe_3S_4$-Pd. However, after the incubation with $Ab_1$, there was a sharp decrease in the signal in curve a, which confirmed that $Ab_1$ was incubated successfully.

Herein, square wave voltammetry (SWV) was used to compare the EC performance of PBG-Au-$Ab_2$ (curve a), PBG-EDC/NHS-$Ab_2$ (curve b) and PBG-GA-$Ab_2$ (curve c). As shown in Fig. 3A, the oxidation peak current of PBG-Au-$Ab_2$ exhibited the highest values. It began to decrease when the cross-linking agent was changed to EDC/NHS. After using GA to link PBG-$NH_2$ and $Ab_2$, a sharp decrease was observed compared with PBG-EDC/NHS-$Ab_2$ (curve b). The obtained result fully confirmed that compared with Au and EDC/NHS, GA could significantly increase the impedance and reduce the conductivity of PBG as an intermediary to connect PBG-$NH_2$ and $Ab_2$.

CV was also used to verify that the signal generated by $Fe_3S_4$-Pd (1.2 mg/mL) on the MGCE was more stable than that on a GCE. As shown in Fig. S4 A, B, it is clear that both of the oxidation peak currents

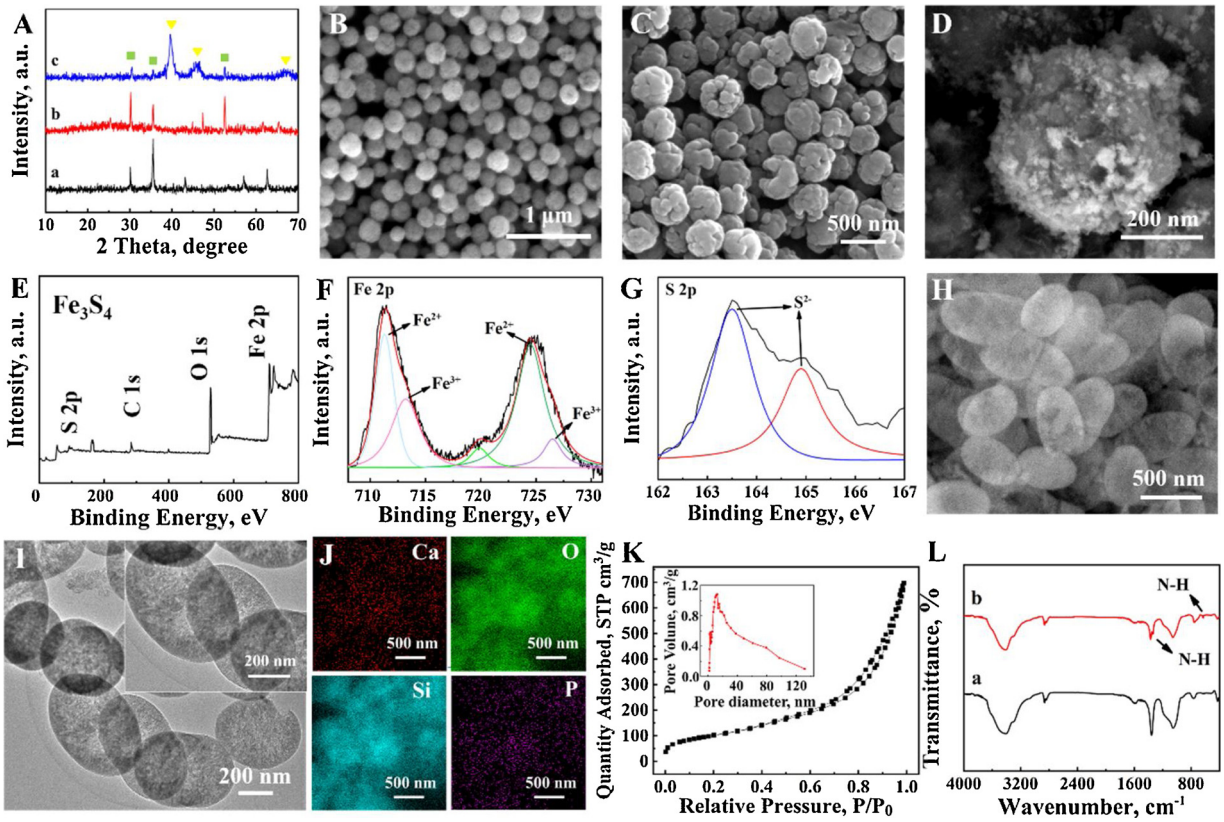


**Fig. 2.** (A) XRD patterns of $Fe_3O_4$ (curve a), $Fe_3S_4$ (curve b) and $Fe_3S_4$-Pd (curve c); SEM images of $Fe_3O_4$ (B), $Fe_3S_4$ (C) and $Fe_3S_4$-Pd (D); XPS spectra of $Fe_3S_4$ (E) in the Fe 2p (F) and S 2p (G) regions; (H) SEM image of PBG; TEM image (I) and energy-dispersive X-ray (EDX) mapping (J) of PBG; (K) $N_2$ adsorption-desorption curves of PBG; FTIR spectrum (L) of PBG (curve a) and PBG-$NH_2$ (curve b).

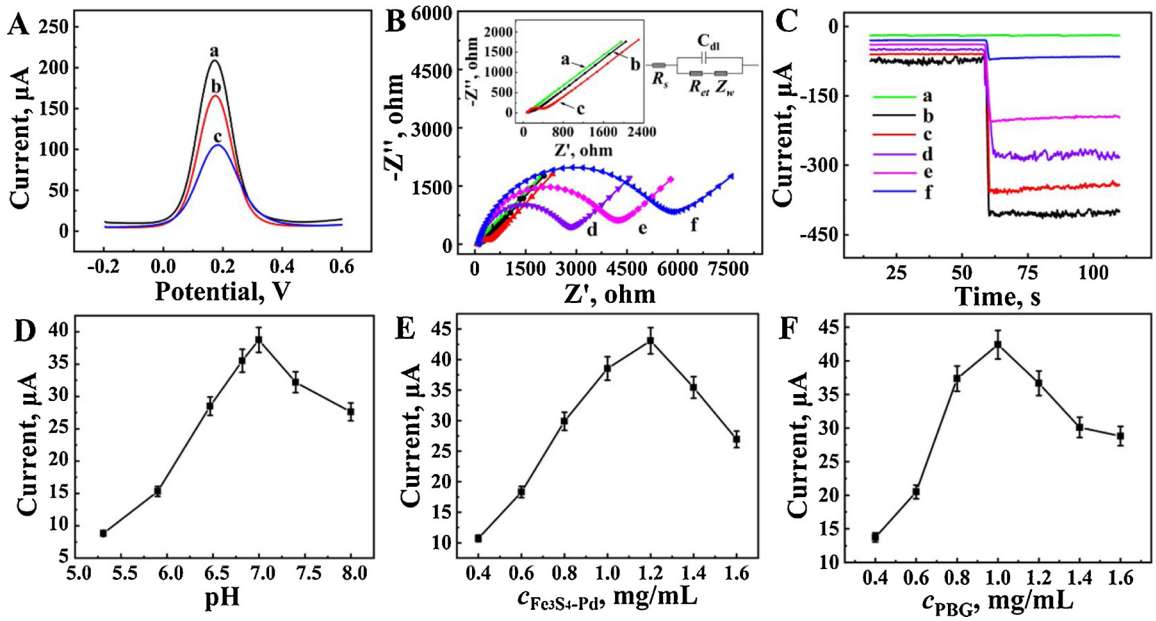


**Fig. 3.** (A) SWV response of PBG-$Ab_2$ using different cross-linking agents: (a) PBG-Au-$Ab_2$, (b) PBG-EDC/NHS-$Ab_2$ and (c) PBG-GA-$Ab_2$; (B) EC impedance spectroscopy (EIS) images derived from the different modified states of the electrodes in $Fe(CN)_6^{3-/4-}$ containing 0.1 mmol/L KCl solution; (C) amperometric *i-t* curve responses at -0.4 V in PBS injected with 5 mmol/L $H_2O_2$, (a) MGCE, (b) $Fe_3S_4$-Pd/MGCE, (c) $Fe_3S_4$-Pd-$Ab_1$/MGCE, (d) BSA/$Fe_3S_4$-Pd-$Ab_1$/MGCE, (e) PCT/BSA/$Fe_3S_4$-Pd-$Ab_1$/MGCE and (f) PBG-$Ab_2$/PCT/BSA/$Fe_3S_4$-Pd-$Ab_1$/MGCE; (D) the effect of pH; (E) the concentration of $Fe_3S_4$-Pd; and (F) the concentration of PBG. Error bars = RSD (n = 5).

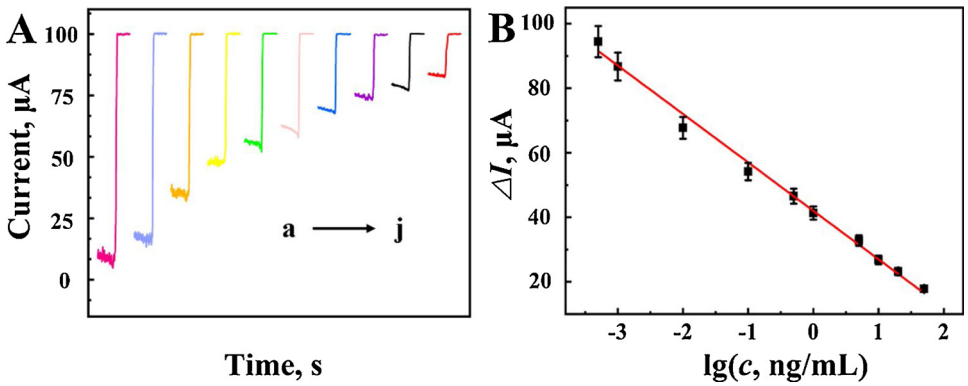


**Fig. 4.** (A) Amperometric *i-t* curve responses and (B) the calibration curve of the EC immunosensor for PCT detection from 500 fg/mL to 50 ng/mL (a ~ j: 0.0005, 0.001, 0.01, 0.1, 0.5, 1, 5, 10, 20, 50 (units: ng/mL PCT)). Error bars = RSD (n = 5).

at sample position number 1, which represented the bare GCE and MGCE, showed almost no difference, demonstrating that both electrodes had similar sensitivities. Later, $Fe_3S_4$-Pd (1.2 mg/mL) was modified on the GCE and MGCE and then they were immersed in PBS for 0 min (2), 3 min. (3) and 5 min. (4). As illustrated in samples 2 ~ 4, it was obvious that for the GCE, with the extension of time, the current response decreased gradually. However, for the MGCE, the current response was almost unchanged. The results confirmed that the magnetic interaction between the MGCE and the magnetic matrix of $Fe_3S_4$-Pd guaranteed that the immunosensor had a higher stability than the $Fe_3S_4$-Pd with the GCE.

### 3.3. EC impedance spectroscopy (EIS) and catalytic characterization

A stepwise self-assembly process and changes in the surface features of the modified MGCE during the assembly process were illustrated by the EIS complex plane (Fig. 3B) of the electrode at different modification phases in a PBS solution containing 0.1 mol/L KCl and 2.5 mmol/L $Fe(CN)_6^{3-/4-}$ [37,38]. Apparently, bare MGCE (curve a) exhibited a very small resistance, which was characteristic of a diffusion-limiting step in the EC process. After the modification with $Fe_3S_4$-Pd (curve b), an increase in impedance was not apparent, revealing the good electric conductivity and excellent electron transfer capacity of $Fe_3S_4$-Pd. However, the obvious increase in the size of the resistance reflected the successful modification of $Ab_1$ (curve c). Subsequently, the gradually increased resistance represented the successful assembly of the added layer of nonconductive BSA biomolecules (curve d). Then, in the presence of the target antigen PCT (curve e), an antibody-antigen interaction caused a continuous increase in the resistance. After PBG-$Ab_2$ was captured on the modified MGCE, a greatly enhanced resistance confirmed the prominent effect that PBG-$Ab_2$ significantly inhibited electron transfer. The series of obtained results demonstrated the successful stepwise self-assembly process of the biorecognition sandwich-type EC immunosensor. Furthermore, to further investigate the impedance, an equivalent circuit diagram of the simulation parameters was used (Table S1).

Similarly, the amperometric *i-t* curve response toward the reduction of $H_2O_2$ (Fig. 3C) was used to further investigate the self-assembly process and electrocatalytic performance of the electrode at different modification phases. There was almost no current change for the MGCE (curve a). Subsequently, owing to the excellent electrocatalytic performance of $Fe_3S_4$-Pd (curve b), it exhibited a sharp increase in the measured current. Because of the steric hindrance effect of PCT $Ab_1$, the current decreased to some extent (curve c), which demonstrated the successful modification of $Ab_1$. The current further decreased with the following modification of nonconductive BSA biomolecules (curve d). After the modification with PCT (curve e) and PBG-$Ab_2$ (curve f), a specific recognition between the PCT antibodies and antigens blocked electron transfer, which caused a continuous decrease in the current.

### 3.4. Optimization of the experimental conditions

First, poor performance was attributed to the recognition between the antigen and antibody being damaged in acidic or alkaline environments; thus, the selection of the optimal pH for the PBS base solution is very important. As shown in Fig. 3D, the maximum signal response was obtained at an optimum pH of 7.4.

Second, because the signal indicator $Fe_3S_4$-Pd catalyzed the reduction of $H_2O_2$ and generated a current signal on the electrode surface, the concentration could directly affect the sensitivity of the immunosensor. From Fig. 3E, we selected 1.2 mg/mL as the optimum concentration of $Fe_3S_4$-Pd.

Moreover, the concentration of PBG should also be considered due to its significant hindrance effect, which affects the sensitivity and EC signal response. Thus, a PBG concentration of 1.0 mg/mL provided the optimal signal throughout this study, as shown in Fig. 3F.

### 3.5. Analytical performance

The proposed sandwich-type EC immunosensor was employed under optimal experimental conditions to detect quantitative concentrations (50 ng/mL ~ 500 fg/mL) of PCT through the amperometric *i-t* curve method, and the response current is shown in Fig. 4A. As exhibited in Fig. 4B, the EC signal response of the logarithmic values of the PCT concentrations was linear within 500 fg/mL to 50 ng/mL, and the linear regression equation of the calibration curve was $\triangle I$ (μA) = 42.00-15.01 log*c* (ng/mL) with a correlation coefficient of 0.991. After further analysis, an ultralow detection limit of 0.13 pg/mL was calculated.

Compared with the previously reported literature listed in Table S2, the proposed sandwich-type EC immunosensor showed a lower detection limit than the other detection methods, which demonstrated its potential in practical applications for detecting PCT.

### 3.6. Reproducibility, selectivity and stability

Reproducibility was measured for the designed sandwich-type EC immunosensor. Herein, five established electrodes, which were incubated with 1 ng/mL PCT, were tested under the same conditions. The experimental measurement results are shown in Fig. 5A, and the relative standard deviation (RSD) of samples 1 ~ 5 was less than 5.0%.

Selectivity also plays a very important role with immunosensors; thus, the selectivity of the proposed immunosensor was also analyzed. Herein, eleven electrodes were prepared. Electrodes 1 ~ 5 were only modified with merely different interference substances, such as prostate-specific antigen (PSA), BSA, carcinoembryonic antigen (CEA), α-

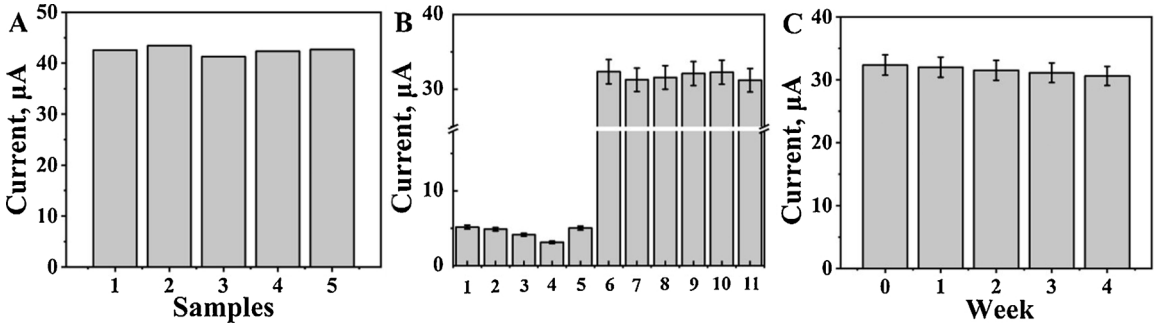


**Fig. 5.** (A) Reproducibility of the immunosensor for the detection of 1 ng/mL PCT. (B) Selectivity testing of the immunosensor: response of the immunosensor to 100 ng/mL PSA (1), 100 ng/mL BSA (2), 100 ng/mL CEA (3), 100 ng/mL AFP (4), 100 ng/mL AA (5), 5 ng/mL PCT (6), 5 ng/mL PCT + 100 ng/mL PSA (7), 5 ng/mL PCT + 100 ng/mL BSA (8), 5 ng/mL PCT + 100 ng/mL CEA (9), 5 ng/mL PCT + 100 ng/mL AFP (10), and 5 ng/mL PCT + 100 ng/mL AA (11), respectively. (C) Stability of the immunosensor. Error bars = RSD (n = 5).

fetoprotein (AFP) and ascorbic acid (AA) (100 ng/mL). Meanwhile, 5 ng/mL PCT was modified on electrodes 6 ~ 11. On this basis, electrodes 7 ~ 11 were modified with 100 ng/mL interference substances respectively. As shown in Fig. 5B, the results demonstrated that the relative standard deviation (RSD) in the current response was less than 5.0% when the immunosensors with an added interference antigen were compared with electrode 6, which did not have an interference antigen. Thus, the selectivity of the immunosensor was acceptable.

To investigate the stability of the proposed immunosensor, some prepared sensors were stored in a refrigerator at 4 °C. One month later, the current response of the sensor detecting 5 ng/mL PCT antigen was less than 5.0% compared to the initial value. As shown in Fig. 5C, the result confirmed the excellent stability of the designed EC immunosensor.

### 3.7. Real sample analysis

To validate the precision and accuracy of the constructed immunosensor and evaluate the feasibility of its practical application, the recovery experiments were used to take a test by a standard addition method. The human serum sample was diluted with a pH 7.4 PBS buffer solution to a level within the calibration range. And after the original concentrations of PCT in the diluted serum samples were confirmed, the standard solutions of PCT antigen were added to the diluted serum samples (adding amounts of 50 pg/mL, 100 pg/mL, 200 pg/mL, 500 pg/mL, and 1000 pg/mL), and the experimental results are shown in Table 1. The RSD of PCT in the serum samples was 3.5 ~ 4.8%, and the recovery range was 97.3 ~ 103% (n = 5), confirming the potential application value of the immunosensor in actual sample detection.

## 4. Conclusion

In summary, a sensitive sandwich-type EC immunosensor was constructed based on a special signal-off mode using $Fe_3S_4$-Pd as a signal indicator and matrix, and functionalized PBG as the label for PCT detection. On the one hand, $Fe_3S_4$-Pd displayed dramatic catalytic properties towards $H_2O_2$ and possessed a strong magnetic interaction with the MGCE, which greatly improved its sensitivity and stability, respectively. On the other hand, the great electron obstruction effect of PBG-$Ab_2$ tremendously promoted the variation in the EC signal difference. Thus, a signal-off-type signal amplification was achieved and further increased the sensitivity. The proposed immunosensor showed a wide linear detection range of 500 fg/mL to 50 ng/mL for PCT, with a low detection limit of 130 fg/mL. Furthermore, the reproducibility, selectivity and stability were all acceptable. All of the above results indicated that the immunosensor could be broadly applied toward the sensitive detection of PCT and even for other disease biomarkers and cells in a clinical diagnosis.

## CRediT authorship contribution statement

**Liu Qu:** Conceptualization, data curation, investigation, visualization, writing - original draft. **Lei Yang:** Formal analysis, methodology. Yong Ren: Formal analysis, methodology. **Xiang Ren:** Supervision, writing - review & editing. **Dawei Fan:** Supervision, writing - review & editing. **Huan Wang:** Supervision, writing - review & editing. **Yueyuan Li:** Conceptualization, formal analysis, methodology, resources. **Huangxian Ju:** Project administration, resources. **Qin Wei:** Exp. project administration, resources and paper revision.

## Declaration of Competing Interest

The authors declare that they have no known competing financial interests or personal relationships that could have appeared to influence the work reported in this paper.

## Acknowledgments

This study was supported by the National Key Scientific Instrument and Equipment Development Project of China (No. 21627809), National Natural Science Foundation of China (Nos. 21607055, 21775053, 21777056), the Natural Science Foundation of Shandong Province (No. 2019GSF111023), Jinan Scientific Research Leader Workshop Project (2018GXRC024), the Innovation team project of colleges and universities in Jinan (No. 2019GXRC027).

**Table 1**
Spike recovery test of PCT in human serum samples.

| Content of PCT in Serum samples (pg/mL) | Addition content (pg/mL) | Detection content (pg/mL) | Average (pg/mL) | RSD (%, $n$ = 5) | Recovery (%) |
|---|---|---|---|---|---|
| 52.01 | 50.00 | 102.20, 100.10, 96.50, 103.20, 106.40 | 101.70 | 3.6 | 99.3 |
| | 100.00 | 150.80, 149.30, 153.20, 161.70, 141.60 | 151.70 | 4.8 | 99.7 |
| | 200.00 | 256.10, 253.40, 230.60, 249.30, 243.50 | 246.60 | 4.1 | 97.3 |
| | 500.00 | 572.30, 563.80, 542.20, 550.90, 597.90 | 565.40 | 3.8 | 102 |
| | 1000.00 | 1129.30, 1059.10, 1108.90, 1097.40, 1034.70 | 1085.90 | 3.5 | 103 |

## Appendix A. Supplementary data

Supplementary material related to this article can be found, in the online version, at doi:https://doi.org/10.1016/j.snb.2020.128324.

## References


[1] M. Singer, C.S. Deutschman, C.W. Seymour, M. Shankar-Hari, D. Annane, M. Bauer, et al., The third international consensus definitions for sepsis and septic shock (Sepsis-3), JAMA 315 (2016) 801–810.

[2] C.W. Goodman, A.S. Brett, Gabapentin and pregabalin for pain-is increased prescribing a cause for concern? N. Engl. J. Med. 377 (2017) 411–414.

[3] C. Wacker, A. Prkno, F.M. Brunkhorst, P. Schlattmann, Procalcitonin as a diagnostic marker for sepsis: a systematic review and meta-analysis, Lancet Infect. Dis. 13 (2013) 426–435.

[4] M. Rieger, C. Kochleus, D. Teschner, D. Rascher, A.K. Barton, A. Geerlof, et al., A new ELISA for the quantification of equine procalcitonin in plasma as potential inflammation biomarker in horses, Anal. Bioanal. Chem. 406 (2014) 5507–5512.

[5] T. Köszegi, Immunoluminometric detection of human procalcitonin, J. Biochem. Biophys. Methods 53 (2002) 157–164.

[6] K. Serebrennikova, J. Samsonova, A. Osipov, Hierarchical nanogold labels to improve the sensitivity of lateral flow immunoassay, Nanomicro Lett. 10 (2018) 24.

[7] S.-H. Wen, X.-L. Zhong, Y.-D. Wu, R.-P. Liang, L. Zhang, J.-D. Qiu, Colorimetric assay conversion to highly sensitive electrochemical assay for bimodal detection of arsenate based on cobalt oxyhydroxide nanozyme via arsenate absorption, Anal. Chem. 91 (2019) 6487–6497.

[8] F. Hong, X. Chen, Y. Cao, Y. Dong, D. Wu, F. Hu, et al., Enzyme- and label-free electrochemical aptasensor for kanamycin detection based on double stir bar-assisted toehold-mediated strand displacement reaction for dual-signal amplification, Biosens. Bioelectron. 112 (2018) 202–208.

[9] Z. Yan, N. Gan, T. Li, Y. Cao, Y. Chen, A sensitive electrochemical aptasensor for multiplex antibiotics detection based on high-capacity magnetic hollow porous nanotracers coupling exonuclease-assisted cascade target recycling, Biosens. Bioelectron. 78 (2016) 51–57.

[10] S. Chen, Y. Lv, Y. Shen, J. Ji, Q. Zhou, S. Liu, et al., Highly sensitive and quality self-testable electrochemiluminescence assay of DNA methyltransferase activity using multifunctional sandwich-assembled carbon nitride nanosheets, ACS Appl. Mater. Interfaces 10 (2018) 6887–6894.

[11] Y. Lv, S. Chen, Y. Shen, J. Ji, Q. Zhou, S. Liu, et al., Competitive multiple-mechanism-driven electrochemiluminescent detection of 8-hydroxy-2'-deoxyguanosine, J. Am. Chem. Soc. 140 (2018) 2801–2804.

[12] Y. Zhang, X. Chen, Nanotechnology and nanomaterial-based no-wash electrochemical biosensors: from design to application, Nanoscale 11 (2019) 19105–19118.

[13] X. Meng, K. Fan, X. Yan, Nanozymes: an emerging field bridging nanotechnology and enzymology, Sci. China Life Sci. 62 (2019) 1543–1546.

[14] L. Yang, Y. Jia, D. Wu, Y. Zhang, H. Ju, Y. Du, et al., Synthesis and application of $CeO_2/SnS_2$ heterostructures as a highly efficient coreaction accelerator in the luminol-dissolved $O_2$ system for ultrasensitive biomarkers immunoassay, Anal. Chem. 91 (2019) 14066–14073.

[15] L. Wang, J. Li, M. Feng, L. Min, J. Yang, S. Yu, et al., Perovskite-type calcium titanate nanoparticles as novel matrix for designing sensitive electrochemical biosensing, Biosens. Bioelectron. 96 (2017) 220–226.

[16] L. Kong, L. Yan, Z. Qu, N. Yan, L. Li, β-Cyclodextrin stabilized magnetic Fe3$S_4$ nanoparticles for efficient removal of Pb(II), J. Mater. Chem. A 3 (2015) 15755–15763.

[17] G. Li, B. Zhang, F. Yu, A.A. Novakova, M.S. Krivenkov, T.Y. Kiseleva, et al., High-purity $Fe_3S_4$ greigite microcrystals for magnetic and electrochemical performance, Chem. Mater. 26 (2014) 5821–5829.

[18] S. Sheng, W. Liu, K. Zhu, K. Cheng, K. Ye, G. Wang, et al., Fe3O4 nanospheres in situ decorated graphene as high-performance anode for asymmetric supercapacitor with impressive energy density, J. Colloid Interface Sci. 536 (2019) 235–244.

[19] L. Chang, A.P. Roberts, A.R. Muxworthy, Y. Tang, Q. Chen, C.J. Rowan, et al., Magnetic characteristics of synthetic pseudo-single-domain and multi-domain greigite ($Fe_3S_4$), Geophys. Res. Lett. 34 (2007) 24304–24309.

[20] A. Paolella, C. George, M. Povia, Y. Zhang, R. Krahne, M. Gich, et al., Charge transport and electrochemical properties of colloidal greigite ($Fe_3S_4$) nanoplatelets, Chem. Mater. 23 (2011) 3762–3768.

[21] Z.H. Yang, S. Ren, Y. Zhuo, R. Yuan, Y.Q. Chai, Cu/Mn double-doped $CeO_2$ nanocomposites as signal tags and signal amplifiers for sensitive electrochemical detection of procalcitonin, Anal Chem 89 (2017) 13349–13356.

[22] L. Gao, K. Fan, X. Yan, Iron oxide nanozyme: a multifunctional enzyme mimetic for biomedical applications, Theranostics 7 (2017) 3207–3227.

[23] Z. Yang, Z. Jian, X. Chen, J. Li, P. Qin, J. Zhao, et al., Electrochemical impedance immunosensor for sub-picogram level detection of bovine interferon gamma based on cylinder-shaped $TiO_2$ nanorods, Biosens. Bioelectron. 63 (2015) 190–195.

[24] H.-C. Ma, J.-L. Kan, G.-J. Chen, C.-X. Chen, Y.-B. Dong, Pd NPs-loaded homochiral covalent organic framework for heterogeneous asymmetric catalysis, Chem. Mater. 29 (2017) 6518–6524.

[25] V. Mazumder, S. Sun, Oleylamine-mediated synthesis of Pd nanoparticles for catalytic formic acid oxidation, J. Am. Chem. Soc. 131 (2009) 4588–4589.

[26] F. He, L. Mi, Y. Shen, T. Mori, S. Liu, Y. Zhang, Fe-N-C artificial enzyme: activation of oxygen for dehydrogenation and monoxygenation of organic substrates under mild condition and cancer therapeutic application, ACS Appl. Mater. Interfaces 10 (2018) 35327–35333.

[27] Y. Yang, F. He, Y. Shen, X. Chen, H. Mei, S. Liu, et al., A biomass derived N/C-catalyst for the electrochemical production of hydrogen peroxide, Chem. Commun. (Camb) 53 (2017) 9994–9997.

[28] A. El-Fiqi, T.H. Kim, M. Kim, M. Eltohamy, J.E. Won, E.J. Lee, et al., Capacity of mesoporous bioactive glass nanoparticles to deliver therapeutic molecules, Nanoscale 4 (2012) 7475–7488.

[29] G.M. Luz, J.F. Mano, Nanoengineering of bioactive glasses: hollow and dense nanospheres, J. Nanopart. Res. 15 (2013) 1457.

[30] I. Ortac, D. Simberg, Y.-s. Yeh, J. Yang, B. Messmer, W.C. Trogler, et al., Dual-porosity hollow nanoparticles for the immunoprotection and delivery of nonhuman enzymes, Nano Lett. 14 (2014) 3023–3032.

[31] J. Zheng, Y. Cao, C. Cheng, C. Chen, R.-W. Yan, H.-X. Huai, et al., Facile synthesis of $Fe_3S_4$ hollow spheres with high-performance for lithium-ion batteries and water treatment, J. Mater. Chem. A 2 (2014) 19882–19888.

[32] Q. Liang, Q. Hu, G. Miao, B. Yuan, X. Chen, A facile synthesis of novel mesoporous bioactive glass nanoparticles with various morphologies and tunable mesostructure by sacrificial liquid template method, Mater. Lett. 148 (2015) 45–49.

[33] Y. Xiao, J.-Y. Hwang, I. Belharouak, Y.-K. Sun, Na storage capability investigation of a carbon nanotube-encapsulated $Fe_{1-x}S$ composite, ACS Energy Lett. 2 (2017) 364–372.

[34] Q. Wu, R. Zhao, W. Liu, X. Zhang, X. Shen, W. Li, et al., In-depth nanocrystallization enhanced Li-ions batteries performance with nitrogen-doped carbon coated $Fe_3O_4$ yolk-shell nanocapsules, J. Power Sources 344 (2017) 74–84.

[35] C. Wang, M. Lan, Y. Zhang, H. Bian, M.-F. Yuen, K. Ostrikov, et al., $Fe_{1-x}S$/C nanocomposites from sugarcane waste-derived microporous carbon for high-performance lithium ion batteries, Green Chem. 18 (2016) 3029–3039.

[36] Y. Zhang, Y. Zhu, G. Lin, R.S. Ruoff, N. Hu, D.W. Schaefer, et al., What factors control the mechanical properties of poly (dimethylsiloxane) reinforced with nanosheets of 3-aminopropyltriethoxysilane modified graphene oxide? Polymer 54 (2013) 3605–3611.

[37] X. Ren, T. Zhang, D. Wu, T. Yan, X. Pang, B. Du, et al., Increased electrocatalyzed performance through high content potassium doped graphene matrix and aptamer tri infinite amplification labels strategy: Highly sensitive for matrix metalloproteinases-2 detection, Biosens. Bioelectron. 94 (2017) 694–700.

[38] T. Zhang, N. Ma, A. Ali, Q. Wei, D. Wu, X. Ren, Electrochemical ultrasensitive detection of cardiac troponin I using covalent organic frameworks for signal amplification, Biosens. Bioelectron. 119 (2018) 176–181.



**Liu Qu** studies in school of chemistry and chemical engineering, University of Jinan as postgraduate student.

**Lei Yang** studies in school of chemistry and chemical engineering, University of Jinan as doctoral student.

**Yong Ren** is a teacher of Department of Mathematical Sciences, Zibo Normal College.

**Xiang Ren** received his B.S. degree in Chemistry of Materials from University of Jinan in 2012, M.S. degree in Chemical Engineering and Technology from University of Jinan in 2015 and Ph.D. degree from University of Jinan/University of Electronic Science and Technology of China in 2019. Now, he is an associate professor in University of Jinan. His main research interests are energy catalysis, nanomaterials controlled-synthesis, and electrochemical biosensors.

**Dawei Fan** received Ph.D. degree from Lanzhou Institute of Chemical Physics, Chinese Academy of Sciences in 2010. Now, she is an associate professor at University of Jinan. Her main research interests are the determination of photoelectrochemical immunosensor.

**Kun Xu** studies in school of chemistry and chemical engineering, University of Jinan as doctoral student.

**Huan Wang** received Ph.D. degree from China university of Geosciences (Beijing). Now, he is an associate professor at University of Jinan. His main research interests are the determination of electrochemical immunosensor.

**Yueyuan Li** is a current Ph. D. student, studies in School of Chemistry and Chemical Engineering, University of Jinan. She is working on constructing immunosensor.

**Huangxian Ju** received his BS, MS and PhD degrees from Nanjing University during 1982–1992. He was a postdoc in Montreal University (Canada) in 1996–1997 and a guest professor in three universities of Germany and Ireland in 1999-2000. He became an associate and full professor of Nanjing University in 1993 and 1999. He is currently the director of State Key Laboratory of Analytical Chemistry for Life Science. His research interests focus on analytical biochemistry, biosensing and molecular diagnosis. He has published 635 papers in different journals with h-index of 85 (Google Scholar h-index 95 with about 31634 citations).